A RECORD OF NEBULAR VS. ASTEROIDAL PROCESSES IN AMOEBOID OLIVINE AGGREGATES FROM KAINSAZ (CO3.2). J. Han[1,2], A. J. Brearley[3], and L. P. Keller[2]. [1]USRA Lunar and Planetary Institute, 3600 Bay Area Boulevard, Houston, TX 77058, USA (jangmi.han@nasa.gov), [2]ARES, NASA Johnson Space Center, 2101 NASA Parkway, Houston, TX 77058, USA, [3]Department of Earth and Planetary Sciences, MSC03-2040, University of New Mexico, Albuquerque, NM 87131,USA.

Introduction: CO3 chondrites show a well-established metamorphic sequence that is correlated with progressive changes in mineralogy, chemistry, and isotopic composition [e.g. 1,2]. These variations with increasing petrologic subtype of CO3s have been attributed to complex, combined processes of fluid-driven metasomatism and thermal metamorphism on their parent body [3], but it is less clear under what conditions these processes occurred.

In CO3s, amoeboid olivine aggregates (AOAs) are very fine-grained and thus sensitive recorders of the effects of metasomatism and metamorphism [4]. Our preliminary TEM study of AOAs in Kainsaz (CO3.2) reported the occurrence of numerous chromite nanoparticles along olivine grain boundaries, which was interpreted as evidence that Cr and Fe were readily redistributed in the presence of fluids during low temperature (<500°C) thermal metamorphism [5]. We have continued our TEM analysis of Kainsaz AOAs to better understand how parent body alteration processes affected AOAs on a micron to submicron scale.

Sample and Methods: A total of 120 AOAs were identified from a ~30 mm^2 thin section of Kainsaz, and four AOAs were studied previously using TEM [5]. For this study, we selected AOA #17 that appears to consist of two separate inclusions due to different degrees of alteration; one region contains all olivine grains with well-developed Fe enrichments along their edge, whereas another has olivine grains only in the outermost region that show Fe enrichments along their edge. We prepared two TEM sections from the edge of these two regions using a FEI Quanta 3D field emission gun SEM/FIB instrument. The FIB sections were then examined in detail using a JEOL 2500SE field emission scanning TEM (STEM) equipped with a Thermo-Noran thin window energy dispersive X-ray (EDX) spectrometer.

Results: *Olivine.* Two FIB sections, 17-A and -B, consist of a compact aggregate of randomly-oriented olivine grains, ~0.5-8.5 μm in size, with well-developed equilibrated grain boundary textures (e.g. straight grain boundaries and 120° triple junctions). Minor pores are present. Individual olivine grains are strongly zoned, but display different ranges of fayalite contents; the fayalite content decreases rapidly over distances of ≤~1 μm from the grain edges towards the interior and then is relatively constant towards their centers.

Chromite. There are various occurrences of chromite ($FeCr_2O_4$) in AOA #17. (1) Abundant, elongated chromite nanoparticles commonly decorate olivine grain boundaries [5], and occasionally crosscut olivine grains. The nanoparticles are all aligned along individual grain boundaries and share the same crystallographic orientation with adjacent olivine. (2) Euhedral chromite grains <1 μm in size occur as inclusions in olivine grains. (3) Pores and cracks are partially filled with chromite. Rarely, needle-like chromite grains grew into pores and are elongated along the a* axis of adjacent olivine (**Fig. 1a**). (4) Chromite lamellae occur in Fe-rich olivine overgrowths at the AOA edge and are oriented parallel to the a* axis of the host olivine overgrowth (**Fig. 1b**). Importantly, we found the same crystallographic orientation relationships from difference occurrences of chromite with respect to olivine: $a_{ol}//(111)_{chr}$, $b_{ol}//[112]_{chr}$, and $c_{ol}//(110)_{chr}$.

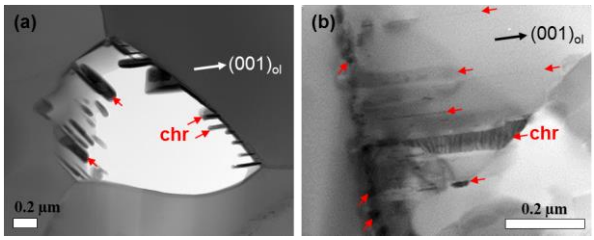

Figure 1. (a, b) Bright-field scanning TEM images of various chromite occurrences in AOA #17.

Pyroxene. In FIB 17-B, olivine grains at the AOA edge are surrounded by diopside and low-Ca pyroxene that display distinct microstructures. Diopside is featureless, but becomes fibrous and intergrown with low-Ca pyroxene in its outermost edge in contact with the matrix. Diopside contains ~1 wt% of both Al_2O_3 and TiO_2 contents. In contrast, low-Ca pyroxene shows irregularities in contrast in bright-field STEM images, and its diffraction patterns show strong streaking parallel to a*. High-resolution TEM imaging revealed disordered 1.35 nm and 1.8 nm spacings intergrown with 0.9 nm (100) spacing of the pyroxene matrix (**Fig. 2**). All these observations indicate the presence of stacking disorders in low-Ca pyroxene, but no associated compositional variations were confirmed by TEM EDX analysis. Low-Ca pyroxene contains ≤1 wt% CaO, but its Fe content increases up to ~4 wt% towards the matrix.

Discussion: The Fe enrichments along individual olivine grain boundaries in Kainsaz AOA #17 are in-

terpreted as an indicator of Mg^{2+}-Fe^{2+} diffusive exchange between AOA olivines and matrix during thermal metamorphism [1,4]. This diffusion appears to be a widespread, but heterogeneous process that resulted in localized variations in the degree of equilibration of Mg^{2+}-Fe^{2+} compositions in olivines from AOAs as well as chondrules [1]. In contrast, a high degree of textural equilibrium observed between olivines, even at the TEM scale, provides evidence for minimal effects of thermal metamorphism on their textures that formed by thermal annealing in the solar nebula [6].

The occurrence of abundant chromite associated with Fe-rich olivine indicates that Fe and Cr were readily redistributed with the onset of thermal metamorphism, probably in the presence of fluids. In addition, different occurrences of chromite share the same crystallographic orientation relationship with respect to olivine, which is a classic relationship between a spinel-structured phase and olivine for a solid-state exsolution process [7]. Therefore, it is possible that chromite formation was structurally controlled by exsolution from (1) primary, forsteritic olivine that formed by high-temperature condensation during thermal metamorphism or (2) secondary Cr-bearing olivine that formed during thermal metamorphism after peak thermal metamorphism. An external source of Fe is required for both olivines, probably from the matrix [4], because olivine in AOAs from ALHA77307 CO3.0 chondrite is nearly pure forsterite with <0.3 wt% FeO [6]. Alternatively, during thermal metamorphism, Cr and Fe were mobile along olivine grain boundaries, but were not readily incorporated into AOA olivine cores, and consequently nanometer-sized chromites grew as individual, isolated grains in an epitactic relationship with the host olivine. These two mechanisms, exsolution and epitaxial growth, may be mutual for the origin of chromite.

The observed microstructural and compositional differences between diopside and low-Ca pyroxene suggest that they behaved differently in response to thermal metamorphism. It appears that the edges of diopside grains were partially replaced by low-Ca pyroxene by the incipient loss of Ca, whereas low-Ca pyroxene underwent Mg^{2+}-Fe^{2+} diffusive exchange with the matrix, to a much lesser degree than olivine [1].

An important question arises as to the formation-conditions of the complex disordered stacking sequence in low-Ca pyroxene. The stacking disorders in low-Ca pyroxene appear as coherent intergrowths of two enstatite polymorphs, monoclinic low clinoenstatite and orthorhombic orthoenstate, in a twin relation [8]. The predominant 0.9 nm spacing represents the *a* dimension of a clinoenstate unit cell. By adding extra 0.45 nm layers parallel to (100), the 1.35 nm spacing corresponds to a single twin in clinoenstatite and the 1.8 nm lattice spacing is double twins in clinoenstatite, eventually producing a orthoenstatite unit cell wide in the *a* direction. These pyroxene microstructures likely result from rapid inversion from primary protoenstatite that formed by high-temperature condensation to twinned clinoenstatite and minor orthoenstatite upon fast cooling [9,10]. On the other hand, orthoenstatite can be produced from clinoenstatite by annealing at ~1000°C [10], but this is highly unlikely given the much lower metamorphic temperatures (<500°C) estimated for Kainsaz [11]. A more careful TEM analysis of the relationship between clino- and ortho-enstatite in low-Ca pyroxene from AOAs is, however, required to better constrain its origin and nature.

Conclusions: Our TEM observations provide lines of evidence for both nebular and parent body processing of olivine and pyroxene in Kainsaz AOAs. In particular, low-Ca pyroxene consists of disordered intergrowths of 0.9 nm clinoenstatite and 1.8 nm orthoenstatite lamellae that may have been transformed from protoenstatite upon cooling after its formation by high-temperature condensation in the solar nebula.

Acknowledge: This study was supported by NASA grants EW14-2-122 to LPK. **References:** [1] Scott E. R. D. & Jones R. H. (1990) GCA 54, 2485-2502. [2] Grossman J. N. & Brearley A. J. (2005) MAPS 40, 87-122. [3] Brearley A. J. & Krot A. N. (2013) In: Metasomatism and the Chemical Transformation of Rock. Lecture Notes in Earth System Sciences. [4] Chizmadia L. J. et al. (2002) MAPS 37, 1781-1796. [5] Han J. & Brearley A. J. (2013) 76th MetSoc, #5155. [6] Han J. & Brearley A. J. (2015) MAPS 50, 904-925. [7] Champness P. E. (1970) Mineral Mag 37, 790-800. [8] Iijima S. & Buseck P. R. (1975) AM 60, 758-770. [9] Smyth J. R. (1974) AM 59, 345-352. [10] Buseck P. R. & Iijima S. (1975) AM 60, 771-784. [11] Cody G. D. et al. (2008) EPSL 272, 446-455.

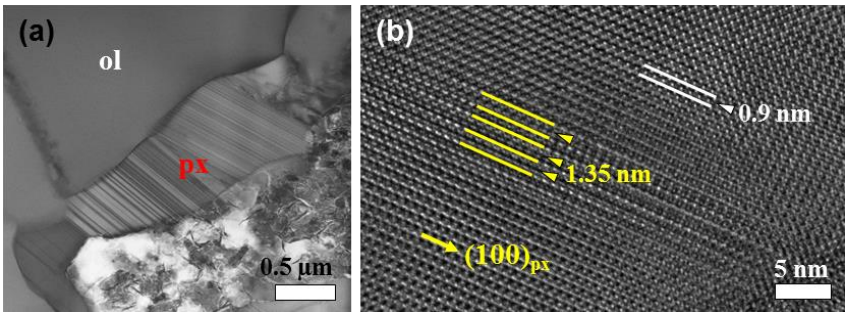

Figure 2. (a) Bright-field scanning and (b) high-resolution TEM images of low-Ca pyroxene that surrounds olivine. In (b), note the disordered presence of 1.35 nm layers in the matrix of 0.9 nm layers parallel to $(100)_{px}$.